Twin lead ballistic conductor based on nanoribbon edge transport

Martin Konôpka and Peter Dieška

SLOVAK UNIVERSITY OF TECHNOLOGY in Bratislava,
Faculty of Electrical Engineering and Information Technology,
Institute of Nuclear and Physical Engineering,
Department of Physics,
Ilkovičova 3, 812 19 Bratislava, Slovak Republic

E-mail: martin.konopka@stuba.sk

31 st March 2017

arXiv:1701.03815v2 [cond-mat.mes-hall] 31 Mar 2017

Abstract

If a device like a graphene nanoribbon (GNR) has all its four corners attached to electric current leads, the device becomes a quantum junction through which two electrical circuits can interact. We study such system theoretically for stationary currents. The 4-point energy-dependent conductance matrix of the nanostructure and the classical resistors in the circuits are parameters of the model. The two bias voltages in the circuits are the control variables of the studied system while the electrochemical potentials at the device's terminals are non-trivially dependent on the voltages. For the special case of the linear-response regime analytical formulae for the operation of the coupled quantum-classical device are derived and applied. For higher bias voltages numerical solutions are obtained. The developed approach allows to study scenarios ranging from independent circuits to strongly coupled ones. The analytical formulae transparently show, among other quantities, how a difference between quasi-Fermi levels of a particular pair of leads can be continuously tuned to a target value including zero. For the chosen model of the GNR with highly conductive zigzag edges we determine the regime in which the single device carries two almost independent currents.

Keywords: multiterminal, conductance, transport, edge, corner, graphene, nanoribbon, chemical potential

1 Introduction

Electronic transport through graphene nanoribbons has attracted attention in particular because their zigzag edges exhibit magnetic properties and support specific modes which

may influence the charge transport [1, 2, 3]. Edges of larger-scale graphene ribbons have been proposed to serve similarly or analogously to optical fibres or waveguides [4]. In experimental works studying electronic transport through a nanoribbon, the flake is typically contacted to electrodes across its whole width, see for instance Ref. [5]. However, if the edges are to be used for the transport, it may be appropriate to make contacts only to the corners of such ribbon. This poses a question if a single graphene nanoribbon or an alternative planar atomistic structure could serve as two wires carrying two independent electric currents. Obviously, there would be some interaction between the currents flowing along the two parallel edges and they would not be fully independent. Still, if the energy ranges of the high density of states, resulting from the zigzag (ZZ) edge modes, are used for the transport, the conductance along the ZZ direction may be significantly larger than the conductance along the perpendicular (armchair, AC) direction. In such case the two ZZ edges might be considered as two relatively independent spatially separated conductors. More generally, such scenario would be the case if the 4×4 conductance matrix of a ribbon preferred one of the directions over the perpendicular and diagonal directions. On the other hand, a nanoribbon with significant conductance along several directions would allow to study the intriguing regime in which the two classical circuits are coupled through the quantum ballistic device. Regardless of the conductance characteristics, such setups would naturally require four electrodes contacted to the corners of the nanoribbon.

Electronic transport through graphene flakes with electrodes contacted at their corners has been studied computationally in the work [6] with focus on non-rectangular flakes such as trapezoids or triangles. The work has addressed the question how the two-contact conductance qualitatively depends on the magnitude of the angles in the two contacted corner areas and on the types of the edges forming the corner. It was in addition found that the usual nearest-neighbor (NN) tight-binding (TB) model was insufficient for proper description of the edge-induced transport properties (provided that the electrodes were attached to the corners).

Four-terminal phase-coherent conductance has been considered by Büttiker [7] in order to clarify the occurrence of asymmetric magnetoresistances. The author considers a sample contacted to two circuits which is a setup similar to the one considered in the present work. On the contrary, the model of Büttiker does not include any classical resistors and is limited to the linear regime. We will return to it in the presentation of our results. Four-terminal schemes have been studied both theoretically and experimentally in setups with two voltage probes implying that two of the four terminals carry zero net currents. Analysis of this specific model can be found as early as in the above cited work by Büttiker. In Ref. [8] an experimental realisation has been described using a one-dimensional single-mode quantum wire. The authors observed vanishing

four-terminal resistance in the wire, in accordance with the theoretical considerations that the resistance of a perfect quantum wire should be zero. A different type of a four-terminal quantum transport device was considered in Ref. [9], with the proposal of using such a device for electron wave computing. Coherent electronic circuits characterised by capacitances in addition to resistances have been studied in the literature. In Ref. [10] violation of Kirchhoff's laws has been experimentally confirmed for a fully coherent quantum resistance-capacitance circuit with the capacitor formed by a quantum dot. A newer review of the coherent RC circuit experimental probing with focus on time-dependent transport can be found in Ref. [11].

In this paper we study a coupled quantum-classical device consisting of a single GNR and of two classical circuits with the four leads contacted to the corners of the GNR. The 4-terminal quantum subsystem is assumed to function in the ballistic regime. The electric currents are driven by DC bias voltage sources in the circuits which include resistors. Transparent analytical formulae displaying the interplay of the quantum and classical elements of the system are derived for both the electric currents as well as the electrochemical or electrostatic potentials in the device's leads. We show that under certain conditions the two electrical circuits of the scheme operate almost independently. Hence such a GNR could serve as two relatively independent conductors which might be found useful in experimental setups and practical applications as it would allow to shrink the device size. The regime in which the circuits are significantly coupled through the ballistic device presents an interesting physical model and is cover by our study as well.

In Sect. 2 we define the system under study. In Sect. 3 we derive main results of our work both for the linear and non-linear regimes. We also provide several details on the quantum-mechanical description of the studied system. In Sect. 4 we apply the theoretical modelling to study the setup defined in Sect. 2. We conclude our results in Sect. 5.

2 The model

The physical model. An atomistic model of one of the considered GNRs is shown in Fig. 1. The red-marked carbon atoms in the corners form the contact areas where the four electrodes (not shown) are attached. If this is accomplished, the whole system in a simple electrical setup can be described by the scheme drawn in Fig. 2. The resistances R_{A} and R_{B} of the two classical resistors are known parameters. The control variables are the static bias voltages V_{A} and V_{B} on the two DC sources, *not* the electrochemical potentials in the leads. The potentials as well as the two currents are unknown non-trivial functions of the bias voltages and have to be determined as it is explained in detail

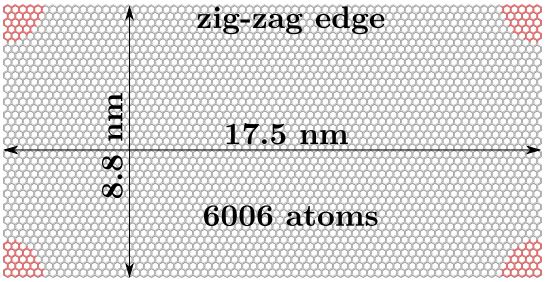

Figure 1: The graphene nanoribbon (GNR) with the four electrodes attached at its corners. Each electrode is modelled by a bunch of 54 identical mono-atomically thin wires [6] (not shown) coupled to the red-marked carbon atoms. Precise GNR dimensions are $L = 71\,b$ (along the ZZ edges) and $W = 62\,a$ (along the AC edges), with $a = 0.142\,\mathrm{nm}$ being the nearest-neighbor distance in graphene and $b = a\sqrt{3}$ the lattice parameter. The GNR is composed of 6006 atoms. In an alternative adapted convention [12] the GNR's dimensions are $(143, 42)$.

below in the text. The stationary regime is assumed for all elements of the scheme. We consider a low-temperature regime in which inelastic scattering of the electrons in the GNR and in its contacts can be neglected. Hence the GNR with its contacts represents a quantum subsystem of the entire scheme. The electronic transport properties of such a contacted device can therefore be described by a 4×4 conductance matrix G. This matrix is computed using a microscopic model described below. For sufficiently low bias voltages the linear regime with $I_\mathrm{A}, I_\mathrm{B} \propto V_\mathrm{A}, V_\mathrm{B}$ can be assumed and the conductance matrix is then considered as energy-independent. This will allow us to derive analytical formulae for currents $I_\mathrm{A}(V_\mathrm{A}, V_\mathrm{B})$ and $I_\mathrm{B}(V_\mathrm{A}, V_\mathrm{B})$ in terms of the fixed system parameters G, R_A, and R_B.

We recall that in the scheme under study (Fig. 2) not only the currents but also the electrochemical potentials μ_2, μ_3 and μ_4 are unknown non-trivial functions, $\mu_\alpha(V_\mathrm{A}, V_\mathrm{B})$, which have to be determined and must strictly be distinguished from the bias voltages. This requirement is dictated by the scheme itself in which even the differences $\mu_2 - \mu_1$ and $\mu_4 - \mu_3$ are *a priori* unknown because the currents through the resistors are unknown. The chemical potential at the terminal 1 is fixed by the ground-level condition. We study also the non-linear regime in which the conductance matrix G is energy dependent.

The microscopic description. We consider GNRs with the electrodes attached to their corners according to Fig. 1. The model of the electrodes and the electronic structure description are similar to those used in Ref. [6] with a notable exception of the more general model of the electrodes in the present work. We use the independent-electron approximation and an extended tight-binding (TB) hamiltonian for the GNR with interactions up to the 3rd NN included. The hopping parameters $t_\mathrm{B} = -2.97\,\mathrm{eV}$, $t'_\mathrm{B} = -0.073\,\mathrm{eV}$ and $t''_\mathrm{B} = -0.33\,\mathrm{eV}$ are taken from Ref. [13]. The orbital overlaps are neglected. The extended interaction range within the GNR was found important to

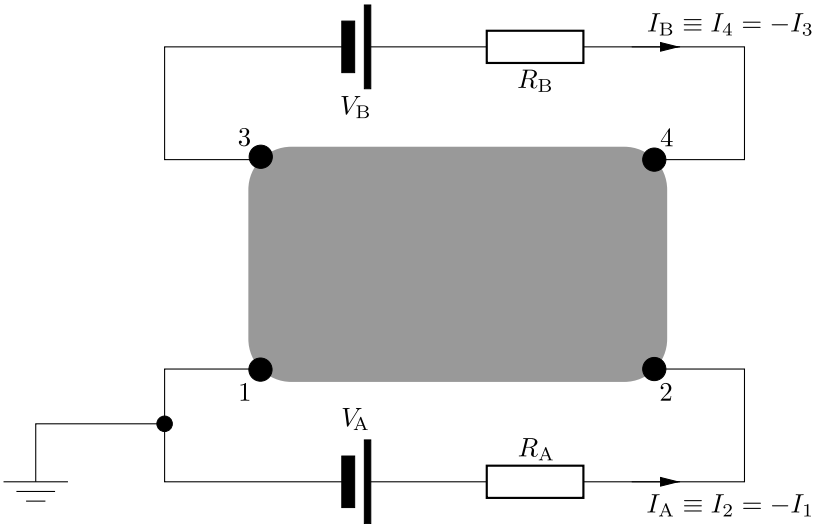

Figure 2: The electric scheme of the considered device. Given control variables are the two bias voltages V_A a V_B. Additional parameters are the classical resistances R_A and R_B and the 4×4, possibly energy-dependent, conductance matrix G of the central ballistic device. Stationary regime is assumed for each element of the scheme. The arrows on the leads mark the conventionally positive directions of the currents I_A and I_B in the circuits.

account for the contributions of the ZZ edge state to the electronic transport if the electrodes are attached to corners of graphene flakes [6]. We do not consider the spin-related effects; the focus of the present work is the description of a four-terminal nanoribbon device coupled to two classical branches of the circuits. A generalisation of our formalism including the spin effects at least on the level of the mean-field approximation to Hubbard hamiltonian would be relatively straightforward although computationally much more expensive [14]. Quantitatively accurate modelling of GNR's electronic structure especially for narrow ribbons would also require an inclusion of the electron-electron interactions into the model [12].

Each electrode in our model is formed by a bunch of mutually non-interacting monoatomically thin wires [15, 6] described within the 2nd NN approximation with the couplings $t_1 = t_B$ and $t_2 = t'_B$. The particular model drawn in Fig. 1 and used for our quantitative analyses employs 54 wires per electrode. Using just a single wire would allow us to study very small currents only. The introduction of the 2nd NN couplings t_2 for the atoms of the wires is the only important modification of the used microscopic theory in comparison to work [6]. The equilibrium on-site (atomic orbital) energies are denoted as ϵ and are assumed to be the same for the entire system, including the electrodes. The extended TB model of the monoatomically thin infinite periodic wires yields the one-electron dispersion relation

$$\mathcal{E}(\mathcal{K}) = \epsilon + \sum_{n=1}^{N_{\mathrm{far}}} 2t_n \cos(n\mathcal{K}) \tag{1}$$

with N_{far} being farthest nearest neighbor considered in the wires; here $N_{\text{far}} = 2$. The dispersion relation can be applied also to the electrons in the semi-infinite wires which the electrodes of our model are composed of. Infinite as well as semi-infinite wire's eigenstates start at the energy $\mathcal{E}_{\text{min}} = \mathcal{E}(0) = \epsilon + 2t_1 + 2t_2$. For typical numerical parameters of the extended TB model the dispersion relation supports eigenstates up to $\mathcal{E}_{\text{max}} = \mathcal{E}(\pi) = \epsilon - 2t_1 + 2t_2$. The Fermi energy of the wires is

$$E_{\text{F}} = \mathcal{E}(\pi/2) = \epsilon - 2t_2 \tag{2}$$

Introduction of the extended TB model of the electrodes thus causes the positive shift $-2t_2$ of the Fermi energy compared to the basic TB model. We note that if the model of the wires was extended up to the 3rd NN, this would have no effect on Fermi energy (2) and overall would have a negligible impact on our results as we have verified in a few calculations. The above defined on-site energy ϵ is the same for all atoms of the system. Its value therefore can be chosen arbitrarily. We use $\epsilon = 2t_2 = 2t'_{\text{B}}$ which results in having $E_{\text{F}} = 0$.

The couplings between the wires and the GNR again extend up to the 2nd NN from the vertex atom of the GNR (the atom of the GNR, to which a given wire is attached). In other words, the vertex atom is coupled to two closest atoms of the semi-infinite wire. Our model assumes the same coupling parameters t_1 and t_2 as defined above for the intra-wire interactions.

3 Theory

3.1 Quantum-mechanical calculations

Standard Green's function formalism (described for instance in Ref. [16]) is used to calculate eigenfunctions of the entire system. Knowledge of the eigenfunctions allows us to compute the transmission and reflection coefficients for electrons incoming from the wires. With the exception of the extended TB model of the wires the calculations have been accomplished according to the route described in Ref. [6]. The Green's function formalism requires knowledge of the semi-infinite wire's eigenstates which are provided in appendix A.

3.2 Landauer-Büttiker formula

We will employ the well-known Landauer-Büttiker (LB) type formula for stationary currents through the leads of a multi-terminal device:

$$I_\alpha = -\frac{2e}{h} \sum_{\substack{\beta=1 \\ \beta\neq\alpha}}^{N_\mathrm{T}} \int_{\mu_\beta}^{\mu_\alpha} \mathcal{T}_{\alpha\leftarrow\beta}(\mathcal{E})\, \mathrm{d}\mathcal{E}\,, \quad \alpha \in \{1, 2, \ldots, N_\mathrm{T}\} \tag{3}$$

N_T is the number of the terminals (also the electrodes), $\mathcal{T}_{\alpha\leftarrow\beta}(\mathcal{E})$ is the transmission coefficient from the terminal β to the terminal α and μ_γ are the electrochemical potentials associated with the individual wires. Formula (3) assumes (i) zero temperature, (ii) the time-reversal symmetry (TRS) and (iii) the trivial description of the spin degrees of freedom (spin degeneracy). The TRS implies that

$$\sum_{\beta(\neq\alpha)} \mathcal{T}_{\alpha\leftarrow\beta}(\mathcal{E}) = \sum_{\beta(\neq\alpha)} \mathcal{T}_{\beta\leftarrow\alpha}(\mathcal{E}) \tag{4}$$

We note that in our model each electrode (attached at its corresponding terminal) is assumed to be composed of a number of the mono-atomically thin wires. We assume that α and β label the electrodes, not the wires. The TRS formula (4) is equally exactly valid for these composite electrodes as it would be valid if the indices α and β labelled the individual wires attached on the central device.

The charge conservation for the central device implies the Kirchhoff's first law:

$$\sum_{\alpha=1}^{N_\mathrm{T}} I_\alpha = 0 \tag{5}$$

The electrochemical potential μ_α at the terminal α is conveniently expressed in terms of the electrostatic potential U_α associated with the terminal (the electrode):

$$\mu_\alpha \equiv -eU_\alpha \tag{6}$$

We recall that in our model (see its description in Sect. 2 and in Fig. 2) the electrochemical potentials themselves as well as the currents are non-trivial unknown functions of the two bias voltages V_A and V_B as will be further explained below.

3.3 Inclusion of the circuits for a 4-terminal device

3.3.1 Formulation of the problem

Consider a device with 4 terminals, i.e. $N_{\mathrm{T}} = 4$ like that drawn in Fig. 2. Each terminal has an electrode connected to it. In our basic statement of the LB formula (3) above the (stationary) currents I_α obey to Kirchhoff's first law (5) and no other constraints were supposed. Now we put in consequences the assumption that the four leads form the two circuits and there are also the two resistors included so that the entire system can be schematically depicted as on Fig. 2. The lower circuit (A) has one of its branches grounded. For such 4-terminal device we have to require the following additional constraining condition,

$$I_3 + I_4 = 0 \tag{7}$$

which is more restrictive than just Kirchhoff's first law (5). We assume the stationary regime for each element of the entire scheme, i.e. also for the sources. Therefore the condition (7) is necessary otherwise an unphysical charge imbalance would be gradually built on the voltage source V_{B} and that would in addition contradict the assumption of the stationarity. The former condition (5) together with the equation (7) then imply a similar condition also on the currents I_1 and I_2:

$$I_1 + I_2 = 0 \tag{8}$$

The presence of the circuits requires that, in addition to the Eqs. (7) and (8), Kirchhoff's second law has to be fulfilled:

$$U_2 = U_1 + V_{\mathrm{A}} - R_{\mathrm{A}} I_{\mathrm{A}}\,, \tag{9a}$$

$$U_4 = U_3 + V_{\mathrm{B}} - R_{\mathrm{B}} I_{\mathrm{B}} \tag{9b}$$

We recall the relation (6): $\mu_\alpha \equiv -eU_\alpha$. According to the scheme in Fig. 2, we can choose

$$U_1 = 0 \tag{10}$$

without any significant loss of generality. This auxiliary setting allows us to accomplish derivations using the potentials U_2, U_3 and U_4 instead of the differences $U_2 - U_1$, $U_3 - U_1$ and $U_4 - U_1$. Hence the three electrostatic potentials U_2, U_3, U_4 and the four currents I_α are unknown quantities and have to be determined as functions of the two given bias voltages V_{A} and V_{B}.

3.3.2 The linearity approximation

Under the assumption of the section's title, the formula (3) for the electric currents takes the frequently accounted form

$$I_\alpha \;=\; \sum_{\substack{\beta=1\\ \beta\neq\alpha}}^{N_\mathrm{T}} G_{\alpha\beta}\,.\,(U_\alpha - U_\beta) \tag{11}$$

We stress again that for the scheme under study (see Fig. 2) the electrostatic potentials U_γ can not be reduced to or confused with the bias voltages V_A and V_B. See also the reasoning in Sect. 2. The linear conductance matrix elements are

$$G_{\alpha\beta} \equiv \frac{2e^2}{h}\,\mathcal{T}_{\alpha\leftarrow\beta} \tag{12}$$

The 4 equations (11) together with the constraints (7), (8) and with the Eqs. (9) form an inhomogeneous set of 8 linear equations with 7 unknowns U_2, U_3, U_4, I_1, …, I_4. Known parameters are the two resistances R_A and R_B, the matrix elements $G_{\alpha\beta}$ satisfying the TRS of the form (4) and the two bias voltages V_A and V_B. I.e. the two voltages V_A and V_B, are supposed to be the control variables in such an experiment, *not* the three electrostatic potentials U_2, U_3, and U_4. There is a linear dependence among the 8 equations. Once the set is properly reduced to remove the dependence, we obtain an inhomogeneous set with a unique solution. The equations are solved in appendix B.1 and resulting linear relations $I_\mathrm{A} = I_\mathrm{A}(V_\mathrm{A}, V_\mathrm{B})$ and $I_\mathrm{B} = I_\mathrm{A}(V_\mathrm{A}, V_\mathrm{B})$ are obtained:

$$I_\mathrm{A} = \frac{\big(\alpha_{\mathrm{AA}} + \gamma R_\mathrm{B}\big)V_\mathrm{A} - \alpha_{\mathrm{AB}} V_\mathrm{B}}{1 + \alpha_{\mathrm{AA}} R_\mathrm{A} + \alpha_{\mathrm{BB}} R_\mathrm{B} + \gamma R_\mathrm{A} R_\mathrm{B}} \tag{13a}$$

$$I_\mathrm{B} = \frac{\big(\alpha_{\mathrm{BB}} + \gamma R_\mathrm{A}\big)V_\mathrm{B} - \alpha_{\mathrm{BA}} V_\mathrm{A}}{1 + \alpha_{\mathrm{AA}} R_\mathrm{A} + \alpha_{\mathrm{BB}} R_\mathrm{B} + \gamma R_\mathrm{A} R_\mathrm{B}} \tag{13b}$$

where

$$\alpha_{\mathrm{AA}} = \frac{1}{S}\,\big[S_1 S - (G_{13} + G_{14})(G_{31} + G_{41})\big] \tag{14a}$$

$$\alpha_{\mathrm{AB}} = \frac{1}{S}\,(G_{13}G_{24} - G_{14}G_{23}) \tag{14b}$$

$$\alpha_{\mathrm{BA}} = \frac{1}{S}\,(G_{31}G_{42} - G_{41}G_{32}) \tag{14c}$$

$$\alpha_{\mathrm{BB}} = \frac{1}{S}\,\big[S_3 S - (G_{31} + G_{32})(G_{13} + G_{23})\big] \tag{14d}$$

and

$$\gamma = \alpha_{\mathrm{AA}}\alpha_{\mathrm{BB}} - \alpha_{\mathrm{BA}}\alpha_{\mathrm{AB}} \tag{15}$$

with

$$S \;=\; G_{13}+G_{23}+G_{14}+G_{24} \;=\; G_{31}+G_{32}+G_{41}+G_{42} \tag{16}$$

and

$$S_\alpha = \sum_{\beta\neq\alpha} G_{\alpha\beta} = \sum_{\beta\neq\alpha} G_{\beta\alpha} = \frac{2e^2}{h}\,(N_\alpha - \mathcal{T}_{\alpha\to\alpha}) \tag{17}$$

N_α is the number of channels per electrode α. In our model its is the number of the elementary wires composing the electrode α. The expressions $\alpha_{CC'}$, S and S_α [see also Eqs. (B.19) and (B.20)], which depend on the quantum conductance matrix elements G only, have been introduced by Büttiker [7] as it will be discussed below.

As stated above, the electrostatic potentials U_α, $\alpha = 2,3,4$, are non-trivial (although linear, under the assumptions of Sect. 3.3.2) functions of the bias voltages on the batteries. Using Eqs. (9), (10) and (13) we first find the potential differences (see also Fig. 2)

$$U_2 - U_1 = \frac{(1+\alpha_{\mathrm{BB}}R_{\mathrm{B}})V_{\mathrm{A}} + \alpha_{\mathrm{AB}}R_{\mathrm{A}}V_{\mathrm{B}}}{1+\alpha_{\mathrm{AA}}R_{\mathrm{A}} + \alpha_{\mathrm{BB}}R_{\mathrm{B}} + \gamma R_{\mathrm{A}}R_{\mathrm{B}}} \tag{18a}$$

$$U_4 - U_3 = \frac{(1+\alpha_{\mathrm{AA}}R_{\mathrm{A}})V_{\mathrm{B}} + \alpha_{\mathrm{BA}}R_{\mathrm{B}}V_{\mathrm{A}}}{1+\alpha_{\mathrm{AA}}R_{\mathrm{A}} + \alpha_{\mathrm{BB}}R_{\mathrm{B}} + \gamma R_{\mathrm{A}}R_{\mathrm{B}}} \tag{18b}$$

restoring in this way the reference potential U_1 which can be set to an arbitrary value and the explicit presence of which allows us to write more general and symmetrical formulae. Next we determine the potentials differences in the perpendicular direction and across the sample. To achieve this goal, we first use the Eq. (B.12a) which yields $U_4 = (I_{\mathrm{A}} - aU_2)/b$ for $U_1 = 0$. U_2 is already know from the Eq. (18a). Accomplishing lengthy algebraic manipulations with multiple use of the TRS relations of the form (3) [see also the Eq. (12)] and finally restoring the reference potential U_1 we arrive at

$$\begin{aligned} U_4 - U_2 = -\frac{1}{SD(G,R)}\,\big[&\big(G_{31}+G_{41}\big)V_{\mathrm{A}} + \big(G_{41}S_3 + G_{31}G_{43}\big)R_{\mathrm{B}}V_{\mathrm{A}} \\ &-\big(G_{13}+G_{23}\big)V_{\mathrm{B}} - \big(G_{23}S_1 + G_{13}G_{21}\big)R_{\mathrm{A}}V_{\mathrm{B}}\big] \end{aligned} \tag{19a}$$

$$\begin{aligned} U_3 - U_1 = \;\;\frac{1}{SD(G,R)}\,\big[&\big(G_{42}+G_{32}\big)V_{\mathrm{A}} + \big(G_{32}S_4 + G_{42}G_{34}\big)R_{\mathrm{B}}V_{\mathrm{A}} \\ &-\big(G_{24}+G_{14}\big)V_{\mathrm{B}} - \big(G_{14}S_2 + G_{24}G_{12}\big)R_{\mathrm{A}}V_{\mathrm{B}}\big] \end{aligned} \tag{19b}$$

(the differences in the perpendicular direction) and

$$U_4 - U_1 = \frac{1}{SD(G,R)}\big[(G_{32}+G_{42})V_\mathrm{A} + (G_{42}S_3 + G_{32}G_{43})R_\mathrm{B}V_\mathrm{A} + (G_{23}+G_{13})V_\mathrm{B} + (G_{13}S_2 + G_{23}G_{12})R_\mathrm{A}V_\mathrm{B}\big] \tag{20a}$$

$$U_3 - U_2 = -\frac{1}{SD(G,R)}\big[(G_{41}+G_{31})V_\mathrm{A} + (G_{31}S_4 + G_{41}G_{34})R_\mathrm{B}V_\mathrm{A} + (G_{14}+G_{24})V_\mathrm{B} + (G_{24}S_1 + G_{14}G_{21})R_\mathrm{A}V_\mathrm{B}\big] \tag{20b}$$

(the potentials differences across the sample). The shorthand notation

$$D(G,R) = 1 + \alpha_{\mathrm{AA}}R_\mathrm{A} + \alpha_{\mathrm{BB}}R_\mathrm{B} + \gamma R_\mathrm{A}R_\mathrm{B} \tag{21}$$

represents the commonly occurring denominator in the above expressions (13) for the currents as well as in the formulae for the differences of the potentials. $D(G,R)$ emerged in the course of the derivation as the determinant of the left hand side of the linear system (B.16). Only one of the four Eqs. (19) and (20) is needed to be derived by the algebraic manipulations. The other three follow from the symmetry of the scheme (Fig. 2) upon performing exchanges of the respective indices and of the bias voltages signs. Although not immediately apparent, the identity

$$(U_2 - U_1) + (U_4 - U_2) + (U_3 - U_4) + (U_1 - U_3) = 0 \tag{22}$$

is obeyed by the results on the right-hand sides of the Eqs. (18a), (19a), (18b) and (19b). The other similar identities which would include the differences $U_3 - U_2$ and $U_4 - U_1$ could also be verified.

The Eqs. (13), (18), (19) and (20) are our main analytical results for the linear regime. The Eqs. (13) transparently show how the currents in the two circuits relate both to the classical and the quantum elements of the scheme. The dependence on the conductance matrix $G_{\alpha\beta}$ is conveniently displayed through the conductances $\alpha_{CC'}$, $C, C' \in \{\mathrm{A}, \mathrm{B}\}$. In the case of vanishing resistances Eqs. (13) simplify to

$$I_\mathrm{A}^{(0)} = \alpha_{\mathrm{AA}}V_\mathrm{A} - \alpha_{\mathrm{AB}}V_\mathrm{B} \tag{23a}$$

$$I_\mathrm{B}^{(0)} = -\alpha_{\mathrm{BA}}V_\mathrm{A} + \alpha_{\mathrm{BB}}V_\mathrm{B} \tag{23b}$$

which is the result found by Büttiker [7].[1] In such case the differences $U_2 - U_1$ and

[1] We note that the voltages V_i in Büttiker's work [7] can not all be chosen arbitrarily and have to satisfy the relation $(T_{21}+T_{41})V_1 - (T_{12}+T_{32})V_2 + (T_{23}+T_{43})V_3 - (T_{14}+T_{34})V_4 = 0$. It is equivalent to the Eq. (B.5) of the present work and follows from the conditions $I_1 = -I_3$ and $I_2 = -I_4$ used in the model of Ref. [7]. Hence the presence of the circuits in the Büttiker's scheme turns one of the electrostatic potentials to an *a priori* unknown quantity which is linearly dependent on the remaining potentials.

$U_4 - U_3$ of the electrostatic potentials would simply be identical to the bias voltages V_A and V_B, respectively, on the batteries, in accordance with the Eqs. (9). The differences in the perpendicular direction and across the sample would remain non-trivial even in the Büttiker's zero resistances model, as can be readily observed from Eqs. (19) and (20). If the resistances are non-vanishing, firstly, the effect of the conductances $\alpha_{CC'}$ on the currents is scaled down by the denominator of the Eqs. (13) which depends not only on the classical resistances but also on the ballistic conductances (the Eq. (21)). Secondly, the additional terms $\gamma R_\mathrm{B} V_\mathrm{A}/D$ and $\gamma R_\mathrm{A} V_\mathrm{B}/D$ influence the currents. Thirdly, the electrostatic (i.e. also electrochemical) potentials adjust their values so that the circuit conditions $I_2 = -I_1$ and $I_4 = -I_3$ are fulfilled.

The Eqs. (19) show that the potentials differences $U_4 - U_2$ or $U_3 - U_1$ can be varied through a continuous range of values by simply tuning the classical resistors in the circuits. For example, employing the Eq. (19a) we can obtain zero difference $U_4 - U_2$:

$$\begin{aligned} &\big[\big(G_{31}+G_{41}\big)+\big(G_{41}S_3+G_{31}G_{43}\big)R_\mathrm{B}\big]V_\mathrm{A} \\ &= \big[\big(G_{13}+G_{23}\big)+\big(G_{23}S_1+G_{13}G_{21}\big)R_\mathrm{A}\big]V_\mathrm{B} \quad \Longrightarrow \quad U_4 = U_2\,, \quad \mu_4 = \mu_2 \end{aligned} \tag{24}$$

[See also the relations (6).] With one of the batteries reversed (for instance $V_\mathrm{B} \to -V_\mathrm{B}$), one can similarly try to set to zero at least one of the potentials differences across the sample as it can be seen from the Eqs. (20). In other words, the differences between the quasi-Fermi levels of the leads can be varied using just tunable resistors in the circuits. An illustration of the effect will be show in Sect. 4.1. The condition like (24) is only achievable for proper combinations of the numerical values of the quantities entering the relation. In many cases the equation would yield a negative resistance R_B.

3.3.3 Special cases formulae

***R* ≪ 1/*G* regime.** In the regime $R_{\mathrm{A,B}} \ll 1/G_{\alpha\beta}$ (here only the off-diagonal matrix elements of G are understood) the terms like $\alpha_{\mathrm{AA}} R_\mathrm{A}$ as well as $\gamma R_\mathrm{A} R_\mathrm{B}$ acquire magnitudes much smaller than unity. The general formulae (13) then can be simplified to a form linear in the resistances:

$$I_\mathrm{A}^{\mathrm{low}R} = I_\mathrm{A}^{(0)} + \alpha_{\mathrm{AB}}\big(\alpha_{\mathrm{BB}} R_\mathrm{B} + \alpha_{\mathrm{AA}} R_\mathrm{A}\big)V_\mathrm{B} - \big(\alpha_{\mathrm{AA}}^2 R_\mathrm{A} + \alpha_{\mathrm{AB}}\alpha_{\mathrm{BA}} R_\mathrm{B}\big)V_\mathrm{A} \tag{25a}$$

$$I_\mathrm{B}^{\mathrm{low}R} = I_\mathrm{B}^{(0)} + \alpha_{\mathrm{BA}}\big(\alpha_{\mathrm{AA}} R_\mathrm{A} + \alpha_{\mathrm{BB}} R_\mathrm{B}\big)V_\mathrm{A} + \big(\alpha_{\mathrm{BB}}^2 R_\mathrm{B} + \alpha_{\mathrm{BA}}\alpha_{\mathrm{AB}} R_\mathrm{A}\big)V_\mathrm{B} \tag{25b}$$

with $I_\mathrm{A}^{(0)}$ and $I_\mathrm{B}^{(0)}$ being Büttiker's currents (23) obtained for the vanishing resistances. As expected, in this situation mainly the quantum conductance limits the currents and the terms linear in R_A and R_B present minor corrections to $I_\mathrm{A}^{(0)}$ and $I_\mathrm{B}^{(0)}$.

***R* ≫ 1/*G* regime.** Such relation between the resistances and conductances usually results in inequalities $\gamma R_\mathrm{A} R_\mathrm{B} \gg \alpha_\mathrm{AA} R_\mathrm{A} \approx \alpha_\mathrm{BB} \gg 1$. Under these assumptions we obtain formulae

$$I_\mathrm{A}^{\mathrm{high}R} = \frac{1}{R_\mathrm{A}} V_\mathrm{A} - \frac{\alpha_\mathrm{AB}}{\gamma R_\mathrm{A} R_\mathrm{B}} V_\mathrm{B} \tag{26a}$$

$$I_\mathrm{B}^{\mathrm{high}R} = \frac{1}{R_\mathrm{B}} V_\mathrm{B} - \frac{\alpha_\mathrm{BA}}{\gamma R_\mathrm{A} R_\mathrm{B}} V_\mathrm{A} \tag{26b}$$

The second terms in these expressions are marginal and apart from the cases of zero V_B or V_A, respectively, they can usually be neglected. Then we get the classical Ohm's formulae $I_\mathrm{A}^{\mathrm{high}R} \approx V_\mathrm{A}/R_\mathrm{A}$ and $I_\mathrm{B}^{\mathrm{high}R} \approx V_\mathrm{B}/R_\mathrm{B}$ as expected in this limit.

Symmetrical conductance matrix, $\mathbf{D_{2h}}$ symmetry. For the device considered in this work (Figs. 2 and 1), apart from few exceptions specified below, the number of independent elements of the conductance matrix is reduced to 4 since we have

$$\begin{aligned} G_{11} &= G_{22} = G_{33} = G_{44} \\ G_{12} &= G_{21} = G_{34} = G_{43} \equiv D \\ G_{13} &= G_{31} = G_{24} = G_{42} \equiv E \\ G_{14} &= G_{41} = G_{23} = G_{32} \equiv F\,. \end{aligned} \tag{27}$$

because of the point-group symmetry and the assumption of zero magnetic flux [7]. We can therefore express the formulae (11), (13) and others for the linear-response regime solely in terms of G_{12}, G_{13}, and G_{14} (and the remaining parameters R_A and R_B). Büttiker's conductances (14) and γ of Eq. (15) simplify to

$$\alpha_\mathrm{AA}^\mathrm{sym} = \alpha_\mathrm{BB}^\mathrm{sym} = D + \frac{E+F}{2} \tag{28a}$$

$$\alpha_\mathrm{AB}^\mathrm{sym} = \alpha_\mathrm{BA}^\mathrm{sym} = \frac{E-F}{2} \tag{28b}$$

$$\gamma^\mathrm{sym} = D^2 + DE + DF + EF \tag{28c}$$

The currents under these higher symmetry conditions can be conveniently expressed in terms of the auxiliary constants $b = F - E$ and $d = 2D + E + F$ as (appendix B.2)

$$I_\mathrm{A}^\mathrm{sym} = \frac{[2d + R_\mathrm{B}(d^2 - b^2)]V_\mathrm{A} + 2bV_\mathrm{B}}{4 + 2d(R_\mathrm{A} + R_\mathrm{B}) + (d^2 - b^2)R_\mathrm{A}R_\mathrm{B}} \tag{29a}$$

$$I_\mathrm{B}^\mathrm{sym} = \frac{[2d + R_\mathrm{A}(d^2 - b^2)]V_\mathrm{B} + 2bV_\mathrm{A}}{4 + 2d(R_\mathrm{A} + R_\mathrm{B}) + (d^2 - b^2)R_\mathrm{A}R_\mathrm{B}} \tag{29b}$$

For the more general case, obeying just the TRS (and not necessarily the symmetries (27)), the constants b and d are given by the expressions (B.13). Corresponding formulae for the electrostatic potentials U_2, U_3 and U_4 of the D_{2h} symmetry device could also be written.

3.3.4 The 4-terminal device beyond the linear response

In this section we provide a generalisation of the considerations in Sect. 3.3.2 beyond the linear regime. It will allow us to more thoroughly describe nano-devices like junctions formed by graphene flakes which are often found to operate in non-linear regimes. The quantum-mechanical part of the system is now parameterised by the matrix $\mathcal{T}$ standing in the Eq. (3) which is now a set of (presumably known) functions of the energy. The energy dependence is the substantial complication in comparison to the linear regime in which the matrix elements were constants. To make the formulae free of numerical prefactors $2e^2/h$, we equivalently use an energy-dependent conductance matrix instead of $\mathcal{T}_{\alpha\leftarrow\beta}(\mathcal{E})$. To keep the dimensions correct, we introduce the auxiliary quantity

$$u \equiv \frac{\mathcal{E}}{e} \tag{30}$$

where $e > 0$ is the unit of charge. The conductance matrix elements are then written as

$$G_{\alpha\beta}(u) \equiv \frac{2e^2}{h}\,\mathcal{T}_{\alpha\leftarrow\beta}(eu) \tag{31}$$

The equations to be solved are (3) with $N_\mathrm{T} = 4$, again with the constraints (7) and (8) and the Kirchhoff's second law Eqs. (9). For convenience we collect and write down all these equations and conditions here, making their specific to the 4-terminal system under study:

$$\begin{aligned}
-\sum_{\substack{\beta=1\\ \beta\neq 1}}^{4} \int_{\mu_\beta/e}^{\mu_1/e} G_{1\beta}(u)\,\mathrm{d}u &= I_1 = -I_\mathrm{A} \\
-\sum_{\substack{\beta=1\\ \beta\neq 2}}^{4} \int_{\mu_\beta/e}^{\mu_2/e} G_{2\beta}(u)\,\mathrm{d}u &= I_2 = +I_\mathrm{A} \\
-\sum_{\substack{\beta=1\\ \beta\neq 3}}^{4} \int_{\mu_\beta/e}^{\mu_3/e} G_{3\beta}(u)\,\mathrm{d}u &= I_3 = -I_\mathrm{B} \\
-\sum_{\substack{\beta=1\\ \beta\neq 4}}^{4} \int_{\mu_\beta/e}^{\mu_4/e} G_{4\beta}(u)\,\mathrm{d}u &= I_4 = +I_\mathrm{B}
\end{aligned} \tag{32}$$

Accompanying relations (9) and (10) for the classical part of the system are now more conveniently expressed in terms of the electrochemical potentials

$$\mu_\alpha \equiv -eU_\alpha \tag{33}$$

rather than the electrostatic ones:

$$\mu_2 = \mu_1 - eV_\mathrm{A} + eR_\mathrm{A}I_\mathrm{A}\,, \qquad \mu_4 = \mu_3 - eV_\mathrm{B} + eR_\mathrm{B}I_\mathrm{B}\,, \qquad \mu_1 \equiv E_\mathrm{F} = 0\,. \tag{34}$$

The accomplish the task we have to solve the coupled set of the above equations (32) and (34), most of them being integral equations. Given parameters and known functions are R_A, R_B, V_A, V_B and $G_{\alpha\beta}(u)$. Main unknown physical quantities to be determined are the currents I_A and I_B. Of secondary interest are the electrochemical potentials μ_α which are also unknown with the exception of μ_1. Obviously, all this is a much more difficult task than it was in the case of its linear counterpart in Sect. 3.3.2. For the non-linear case we develop a numerical algorithm which takes μ_2, μ_3, μ_4, I_A and I_B as unknown functions of the two independent (and presumably experimentally controllable) variables V_A and V_B. As the key part of the derivation, we express the coupled set of the equations (32) and (34) also at varied values $V_\mathrm{A} + \delta V_\mathrm{A}$ and $V_\mathrm{B} + \delta V_\mathrm{B}$ of the bias voltages. Resulting dependent variables are $\mu_\alpha(V_\mathrm{A}+\delta V_\mathrm{A}, V_\mathrm{B}+\delta V_\mathrm{B}) = \mu_\alpha(V_\mathrm{A}, V_\mathrm{B}) + \delta\mu_\alpha$, $\alpha \in \{2,3,4\}$, and analogously for the currents. This differentiation leads to a set of algebraic equations of the form (9), (B.1), (B.2), (B.3), and (B.4), where instead of the variables stand their differentials. Several details of this procedure are provided in appendix C.

We briefly return to the Landauer-Büttiker type formula (3). In calculations beyond the equilibrium the spectra of the transmission coefficient should be evaluated at given set of electrochemical potentials $\mu_1, \ldots, \mu_4$, in short μ: $\mathcal{T}_{\alpha\leftarrow\beta} = \mathcal{T}_{\alpha\leftarrow\beta}(\mathcal{E};\mu)$. As μ's depend non-trivially on chosen bias voltages V_A and V_B, we do not have any *a priori* knowledge of μ in our quantum-mechanical (QM) calculations of $\mathcal{T}_{\alpha\leftarrow\beta}(\mathcal{E};\mu)$ apart from $\mu_1 \equiv E_\mathrm{F} = 0$ due to the ground-level condition. To make an approximation to a full non-equilibrium calculation we therefore proceed in five steps: (1) We obtain $\mathcal{T}_{\alpha\leftarrow\beta}(\mathcal{E};\mu)$ with all μ's set to E_F like we did in the low-voltage calculation. We briefly denote these coefficients as $\mathcal{T}^{(0)}$. (2) We accomplish circuit calculations by solving the set of the Eqs. (32) and (34) using $\mathcal{T}^{(0)}$. In this manner we obtain dependences $\mu^{(1)}(V_\mathrm{A}, V_\mathrm{B})$, $I_\mathrm{A}^{(1)}(V_\mathrm{A}, V_\mathrm{B})$, and $I_\mathrm{B}^{(1)}(V_\mathrm{A}, V_\mathrm{B})$ as a first approximation on chosen domains $V_\mathrm{A} \in [0, V_\mathrm{max}]$ and $V_\mathrm{B} \in [0, V_\mathrm{max}]$. (3) Assuming that in further search we seek for refined $\mu^{(2)}(V_\mathrm{B})$, $I_\mathrm{A}^{(2)}(V_\mathrm{B})$, and $I_\mathrm{B}^{(2)}(V_\mathrm{B})$ at a *fixed* value of V_A, we take the values $\mu_\alpha^{(1)}(V_\mathrm{A}, V_\mathrm{max}/2)$ as new reference electrochemical potentials. (4) These new reference – now non-equilibrium – settings are used for the next QM calculation of $\mathcal{T}_{\alpha\leftarrow\beta}(\mathcal{E};\mu)$, now denoted as $\mathcal{T}^{(1)}$.

(5) $\mathcal{T}^{(1)}$ is used in repeated circuit calculations (again solving the Eqs. (32) and (34)) thus yielding more accurate results $\mu(V_\mathrm{B})$, $I_\mathrm{A}(V_\mathrm{B})$, and $I_\mathrm{B}(V_\mathrm{B})$, now assumed to be valid for the chosen V_A only. The refined quantities still do not present full non-equilibrium results. They are however a significantly better approximation than the results obtained for the equilibrium spectra of $\mathcal{T}$'s. We find that the differences of $I_\mathrm{A}(V_\mathrm{B})$, and $I_\mathrm{B}(V_\mathrm{B})$ between the first and second approximation are up to 10%.

4 Application to graphene nanoribbons

We provide an illustrative set of results for the nanoribbon junction draw in Fig. 1.

4.1 Linear-response regime at the neutrality point

In this regime very low bias voltages are assumed. Using the microscopic approach described in Sect. 2 we obtain numerical values of the linear conductance of the particular GNR shown in Fig. 1. The quantum subsystem of the whole scheme (Fig. 2) – the GNR with its four contacts – provides a purely ballistic transport as we assume zero temperature. Its electronic transport properties at the equilibrium Fermi level can be represented by the matrix of the transmission coefficients $\mathcal{T}^\mathrm{eq}$ or alternatively in terms of the corresponding conductance matrix G^eq as following from the Eq. (12):

$$\mathcal{T}^\mathrm{eq} = \frac{G^\mathrm{eq}}{G_0} \approx \begin{pmatrix} 53.51 & 0.1840 & 0.1246 & 0.1816 \\ 0.1840 & 53.51 & 0.1816 & 0.1246 \\ 0.1246 & 0.1816 & 53.51 & 0.1840 \\ 0.1816 & 0.1246 & 0.1840 & 53.51 \end{pmatrix} \tag{35}$$

where $G_0 = 2e^2/h$ is the conductance quantum. The large diagonal matrix elements can easily be understood for they mainly represent transmissions of the incoming electrons back to the wires belonging to the same electrode. In our model (Fig. 1) we assume 54 (monoatomically thin) wires per electrode, in other words 54 conductance channels per electrode. In terms of $\mathcal{T}$, any incoming electron close to the Fermi level is most likely transmitted to a wire belonging to the same electrode which is the reason that the cumulative diagonal elements are all close to 54. Nevertheless, the net effect of the diagonal elements is zero in accordance with the Eq. (3). The ordering of the matrix elements is given by the indices $1, \ldots, 4$ at the contacts of the GNR as defined in Fig. 2. The matrix is symmetric (although no symmetry was forced in the calculation). Below we omit writing the superscript eq at G.

In our first computational analysis of the entire scheme we use resistances $R_\mathrm{A} = 7.3 \cdot 10^{-5}\,\hbar/e^2 \approx 0.3\,\Omega$ and $R_\mathrm{B} = 4.9 \cdot 10^{-5}\,\hbar/e^2 \approx 0.2\,\Omega$. A typical or roughly an average

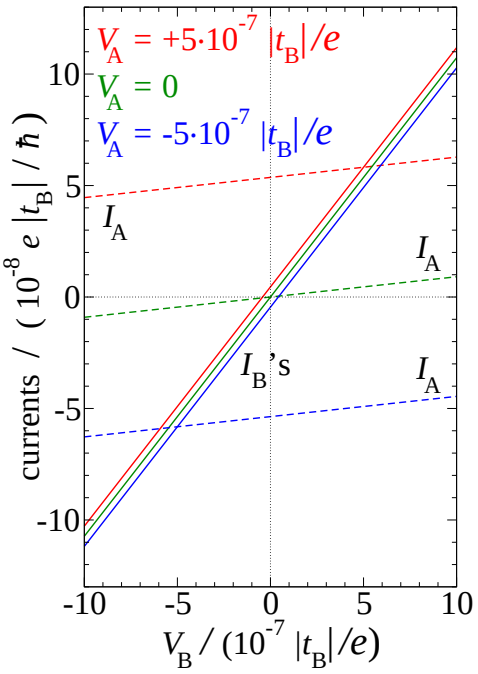

Figure 3: Illustration of the result in the linear regime for the GNR junction shown in Fig. 1 and forming the two-circuit device according to Fig. 2. The results show how the currents in the circuits A and B vary with $V_{\rm B}$ at the three fixed values of $V_{\rm A}$. The resistors used in the circuits have values $R_{\rm A} = 7.3 \cdot 10^{-5}\,\hbar/e^2 \approx 0.3\,\Omega$ and $R_{\rm B} = 4.9 \cdot 10^{-5}\,\hbar/e^2 \approx 0.2\,\Omega$. The natural voltage unit $|t_{\rm B}|/e \approx 2.97\,{\rm V}$, e being the unit charge and $t_{\rm B}$ the graphene nearest-neighbor hopping parameter. The used conductance matrix is specified by the Eq. (35). In SI units the voltage $V_{\rm B}$ scales up to 2.97 µV while the currents axis scales up to 94 pA.

value of the off-diagonal matrix elements of the equilibrium-level conductance (35) is $G^{\rm off} \approx 0.16\,G_0 \approx 0.05\,e^2/\hbar$. The choice of the resistances then correspond to the regime $R \ll 1/G^{\rm off}$, i.e. with the classical conductances much higher than those of the quantum subsystem. The results are conveniently visualised in terms of currents and are shown in Fig. 3. The tiny magnitudes of the bias voltages and consequently of the currents (below 100 pA) ensure the strictly linear regime. From the figure we see that the current through circuit B is weakly influenced by the current in circuit A. In other words, the two circuits influence each other to a minor although noticeable extent. The seemingly simple, almost independent operation, of the two circuits is in fact a results of a cancelation of internal currents flowing inside the GNR between its terminals. This can be easily understood using the formulae for the currents, conveniently starting from the Eqs. (29) valid for the considered symmetric junction. Because the parameters used for Fig. 3 satisfy the conditions $R_{\rm A,B} \ll 1/G_{\alpha\beta}$, we can neglect the resistances which leaves us with the currents approximately expressed by Büttiker's formulae (23), now written for the sample of the D_{2h} symmetry:

$$I_{\rm A} \approx I_{\rm A}^{(0,{\rm sym})} = \frac{1}{2}(d\,V_{\rm A} + b\,V_{\rm B})\,, \qquad I_{\rm B} \approx I_{\rm B}^{(0,{\rm sym})} = \frac{1}{2}(d\,V_{\rm B} + b\,V_{\rm A}) \tag{36}$$

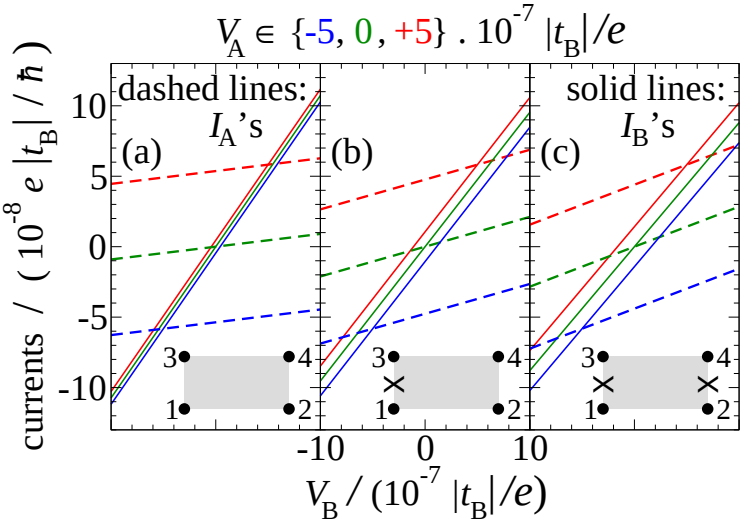

Figure 4: I_A, I_B vs. V_B plots illustrating the impact of the edge disorder on the device operation. The quantities on the axes as the same as in Fig. 3, as well as the axes scalings and color coding. The scheme of the device is illustrated in Fig. 2. Pane (a) corresponds to the situation with the perfect GNR as in Fig. 1 and repeats the results taken from Fig. 3. Pane (b) shows results for a junction with a blocked transport along the (presumably disordered) AC edge. This is numerically represented by practically vanishing $G_{13} = G_{31} \approx 0.003\,G_0 \ll G_{12}$ matrix elements while keeping the other matrix elements the same as in the Eq. (35). All other conditions are identical to those used for graph (a). Pane (c) displays such linear I/V plots for a GNR with both AC edges blocking the transport which is quantified by the tiny quantity $G_{24} = G_{42} \approx 0.003\,G_0$ in addition. The insets provide condensed information on the junction orientation and the labelling of its contacts (c.f. Fig. 2). The X crosses on the insets mark the channels blocking the electronic transport.

The second of them can in terms of the parameters (27) be expressed as

$$I_B \approx I_B^{(0,\mathrm{sym})} \approx \frac{1}{2}\left[(2D + E + F)V_B + (F - E)V_A\right] \tag{37}$$

The term responsible for the mutual interaction of the two circuits is thus proportional to $F - E \equiv G_{14} - G_{13}$ which is a very small quantity compared to term $2D + E + F \equiv 2G_{12} + G_{13} + G_{14}$ as can be judged from the matrix (35). Because E and F are of similar magnitudes, they partially cancel each other: there is a partial cancelation of the currents flowing along the AC edges and the currents across the diagonal of the GNR.

Electrical conductance properties of GNRs can be affected by different kinds of defects. For example, the conductance of GNRs with the current flowing along their AC edges can be destroyed by the AC edge disorder [17]. If the magnitude of the matrix elements G_{13} and G_{24} (or only one of them) is lowered due to the defects or due to any designed feature, the currents in the two circuits would become influencing each other in a more significant extent. We provide a semi-quantitative representation of these effects in Fig. 4 for which we assume [Fig. 4(b)] $G_{13} \ll G_{12}, G_{14}, G_{24}$ or similarly also [Fig. 4(c)] $G_{13}, G_{24} \ll G_{12}, G_{14}$. The equalities $G_{12} = G_{34}$ and $G_{14} = G_{23}$ still hold for all results

in the figure. In particular, we employ the numerical value $G_{13} = 0.001\, e^2/\hbar \approx 0.003\, G_0$ and the same for G_{24} in the (c) case. This is a practically vanishing quantity when compared to G_{12} as well as to G_{23}. The other matrix elements $G_{\alpha\beta}$ for the purpose of a defect impact modelling remain unchanged, i.e. they are given by Eq. (35). Our description of the edge disorder (or other defects) impact is qualitative because we do not compute the conductance matrix for a disordered sample. Instead we only define its matrix elements as stated above and perform the calculations of the currents [18]. Especially the pane (c) of Fig. 4 demonstrates the regime in which the two classical circuits substantially interact through the quantum device. We note that the special-case equations (27) – (29) can not be applied to scenario (b). The general formulae (13) must be used instead.

As it can be directly observed from the results of Sect. 3.3.2, the effects of the resistors are significant and most interesting in the regime with the resistances of the magnitudes $R \approx 1/G^{\mathrm{off}}$ (semi-quantitatively). Employing a tunable resistor (or both of them) in this regime, one can balance the quasi-Fermi levels (6) of a certain pair of the leads provided that the remaining physical parameters permit it. One particular scenario is described by the Eq. (24). An illustration of the effect is shown in Fig. 5 in which the currents and the potentials differences are plotted as given by the Eqs. (13), (18), (19) and (20). We choose $R_{\mathrm{A}} = 7.3\, \hbar/e^2 \approx 30.0\, \mathrm{k\Omega}$. The bias voltages on the sources use the values $V_{\mathrm{A}} = 2.5 \cdot 10^{-7}\, |t_{\mathrm{B}}|/e \approx 0.74 \cdot 10^{-6}\, \mu\mathrm{V}$ and $V_{\mathrm{B}} = 2.6 \cdot 10^{-7}\, |t_{\mathrm{B}}|/e \approx 0.77 \cdot 10^{-6}\, \mu\mathrm{V}$. The electrostatic potentials of the leads 2 and 4 match at the value $R_{\mathrm{B}}^{\mathrm{match}} = 7.936\, \hbar/e^2 \approx 32.6\, \mathrm{k\Omega}$; at this value the solid dark green curve crosses zero thus indicating the equality $U_2 = U_4$. Because of the high symmetry of the studied sample, the potentials U_1 and U_3 (the solid blue plot) are balanced at the same value of R_{B}.

4.2 Beyond the linear response

If the magnitude one or both of the bias voltages V_{A} and V_{B} is increased above a certain threshold (around $10^{-4}\, |t_{\mathrm{B}}|/e$ in our model), the electrochemical potentials μ_2, μ_3, and μ_4 may take values such that the electrons most relevant for the transport acquire energies from the range of the ZZ edge modes.[2] Conductance matrix $G_{\alpha\beta}$ is strongly energy-dependent in this energy window. Associated theory and the computational procedure have been provided in Sect. 3.3.4 and its appendix C. The non-linear regime is reached as soon as the matrix elements $G_{\alpha\beta}$ vary significantly with energy between the integration bounds of the Eqs. (32). Fig. 6 shows the spectra of the matrix elements computed under the equilibrium conditions; we note that such spectra computed under

[2] Particular values of the electrodes' electrochemical potentials at which the ZZ-edge modes are probed depend on an applied gate voltage which can effectively shift the energy levels of the central device. Apart from Sect. 4.3 zero gate voltage is assumed.

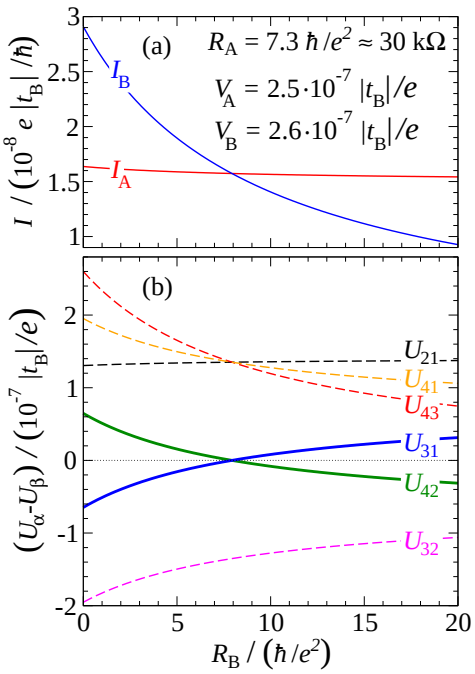

Figure 5: Illustration of the leads' quasi-Fermi level balancing using a tunable resistor and of the other linear-regime results. The electric currents (a) and the electrostatic potentials differences $U_{\alpha\beta} \equiv U_\alpha - U_\beta$ (b) resulting from the formulae (13), (18), (19) and (20) are plotted as functions of the resistance R_B. The resistance R_A and the bias voltages V_A and V_B remain fixed at their values typed within the upper pane. The quantum subsystem is the same GNR as it was assumed for Figs. 3 and 4 (a). The conductance properties of the quantum subsystem are described by the matrix (35). The figure illustrates mainly the regime of (semi-quantitatively) $R \approx 1/G^\mathrm{off}$, where G^off is a typical value of a non-diagonal element of the conductance matrix. The thick green curve crosses the zero value [marked by the horizontal dotted lined in pane (b)] which indicates that at that point $U_2 = U_4$ or that the electrochemical potentials at leads 2 and 4 match (see also Fig. 2). Due to the high symmetry of the studied GNR the potentials U_1 and U_3 match at the same value of R_B. For conversions to SI units the value of $|t_\mathrm{B}| \approx 3\,\mathrm{eV}$ should be used as specified in the text.

non-equilibrium conditions would have quite similar shapes, exhibiting mostly just shifts along the energy axis compared to the equilibrium case. The green line shows the matrix elements strongly affected by the presence of the zigzag edges of the GNR. The sharp oscillations due to the ZZ-edge modes contribute to the currents and make them non-linear with the increasing chemical potentials as well as with the increasing bias voltages V_A and V_B. The oscillations start at energies as low as about $8\cdot10^{-5}\,|t_\mathrm{B}|$ above the equilibrium Fermi level meaning that the transport becomes non-linear even for such relatively low bias voltages. A linear regime for higher biases would be possible upon application of a proper gate voltage on the GNR which would shift the peaks away from the equilibrium Fermi level.

The currents itself are displayed in Fig. 7 as functions of the bias voltage V_B for three fixed values of V_A. They have been obtained in the five-steps procedure described at the end of Sect. 3.3.4, i.e. they include the partial correction due to the non-equilibrium

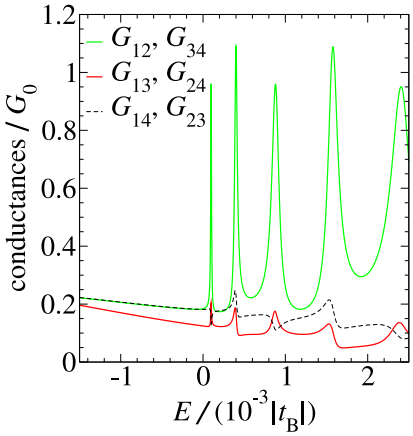

Figure 6: The elements of the conductance matrix $G_{\alpha\beta}$ expressed in the units of the conductance quantum as functions of the energy $\mathcal{E}$ for the nanoribbon shown in Fig. 1. They have been calculated under the equilibrium conditions. Their values at $\mathcal{E} = 0$ are given by the Eq. (35).

conditions. Pane (a) of the figure presents results for the low-resistance regime in which $R_A, R_B \ll G^{edge}$, with $G^{edge} \approx 0.5\,G_0$ being a typical magnitude of the off-diagonal matrix elements $G_{12} = G_{34}$ of the conductance matrix on the examined interval of energies. These matrix elements describe the transport along the ZZ edges. As expected, with increased resistances the currents become lower as well as the impact of the non-linearities in the conductance matrix spectra (pane (b) of Fig. 7).

An overall dependence on the resistance (with the fixed ratio $R_A/R_B = 7.3/4.9$) is semi-quantitatively displayed in Fig. 8 using black line with circles. Here the value of R used for the descriptions of the horizontal axis is the arithmetic average between R_A and R_B. I_{max} on the vertical axis is the maximum chosen among the currents I_A and I_B for given R_A and R_B on the examined domain of the bias voltages: $V_A \in \{0,\ 2\cdot 10^{-3}\,|t_B|/e\}$, $V_B \in [0,\ 2\cdot 10^{-3}\,|t_B|/e]$. The value of G^{edge} typed within the graph serves only for comparison purposes, i.e. what is the actual resistance R in comparison to the typical inverse conductance of the ZZ edge. For another comparison, in the same graph we in addition provide results for the linear regime (the smooth red line). They were calculated using the Eqs. (29) with the conductance matrix (35) and $V_A = V_B = 2\cdot 10^{-3}\,|t_B|/e$. These bias voltages are too high for the linear regime but still the results calculated in this way (solid red line in Fig. 8) present a convenient analytically obtained reference to the numerical results for the non-linear regime (the black plot with circles).

4.3 Resonantly increased conductance in the linear regime

In Sect. 4.1 the impact of the suppressed conductances G_{13} and G_{24} was semi-quantitatively examined in the low-voltage regime around the neutrality point of the studied model (Fig. 4). The suppression of the conductance (of the AC edges) may occur as a conse-

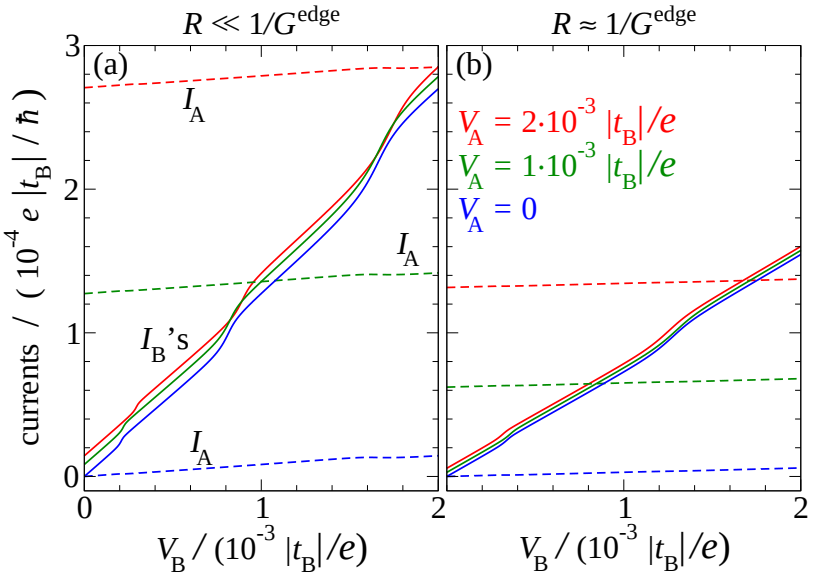

Figure 7: Similar to Fig. 3 but now for the non-linear regime. Pane (a) shows results for the low resistances $R_A = 7.3 \cdot 10^{-5}\,\hbar/e^2$ and $R_B = 4.9 \cdot 10^{-5}\,\hbar/e^2$ which is qualitatively marked as $R \ll 1/G^{\text{edge}}$. Pane (b) shows analogous results for five orders of magnitude larger resistances $R_A = 7.3\,\hbar/e^2$ and $R_B = 4.9\,\hbar/e^2$ which is marked as the regime $R \approx 1/G^{\text{edge}}$. The color coding and the description inside the panes is the same for both graphs.

quence of certain edge defects [17, 18]. The *effectively* almost independent conductance channels (Fig. 4(a)) along the two ZZ edges then turn to the significantly coupled ones (Fig. 4(b,c)).

To achieve a regime of the relatively independent current flows along the ZZ edges regardless of possible disorder of the AC edges, the conductance along the ZZ edges should be increased. This can be reached using resonant transport conditions under which the ZZ edge modes are employed. The conductance matrix (35) has been calculated under the non-resonant conditions, i.e. such that the relevant energies of the incident electrons have not been tuned to the ZZ edge-mode resonances. Such tuning can be obtained using a proper gate potential applied to the GNR while still working with tiny bias voltages, i.e. in the linear regime. The effect of such a gate voltage is to shift the spectra displayed in Fig. 6. In this way, upon applying a shift $-0.0016\,|t_B|$ to the spectra,[3] we can work with the conductance matrix

$$\mathcal{T}^{\text{res}} = \frac{G^{\text{res}}}{G_0} \approx \begin{pmatrix} 52.75 & 1.012 & 0.07975 & 0.1568 \\ 1.012 & 52.75 & 0.1568 & 0.07975 \\ 0.07975 & 0.1568 & 52.75 & 1.012 \\ 0.1568 & 0.07975 & 1.012 & 52.75 \end{pmatrix} \tag{38}$$

[3] I.e. we do not perform an explicit quantum-mechanical calculation with an applied gate voltage; such a calculation would provide us with a matrix G practically the same as the one obtained by the simple shift of the spectra calculated for zero gate voltage.

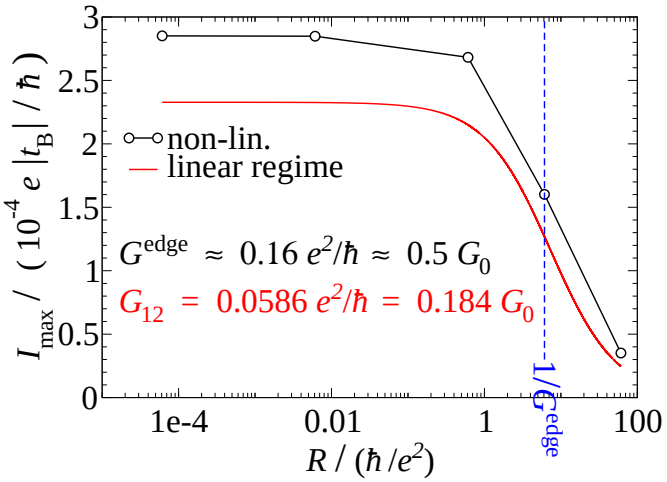

Figure 8: Black line with circles: maximum of any of the currents I_A and I_B versus resistance. The maxima are determined on the chosen domain of the bias voltages, $V_A \in \{0,\ 2\cdot10^{-3}\,|t_B|/e\}$, $V_B \in [0,\ 2\cdot10^{-3}\,|t_B|/e]$, again for the GNR shown in Fig. 1. The resistance R is the arithmetic average of the R_A and R_B resistances which are always chosen in the same ratio $R_A/R_B = 7.3/4.9$. G^{edge} is a typical G_{12} or G_{34} conductance value along the ZZ edges such as can be seen also in Fig. 6. The vertical dashed line marks the value of $1/G^{edge}$ on the resistance axis. For comparison, analytical results for the linear regime are outlined with the smooth red line. They have been calculated using the formulae (29) and the conductance matrix (35).

which should be contrasted to the matrix (35) obtained for the neutrality point. Again, a graphical representation of these results in terms of the currents is used: we prepare the three-pane Fig. 9 in the same style as Fig. 4. We use the same values of the bias voltages for easier comparison. Resistances R_A and R_B are also the same as used for Figs. 3 and 4. The vertical axes are now scaled up to higher values resulting predominantly from the resonantly increased matrix elements G_{12} and G_{34}. Pane (a) of Fig. 9 shows results for the intact GNR (Fig. 1). In panes (b) and (c) we provide semi-quantitative results under the assumption that one or both AC edges block current transport, in full analogy with Fig. 4. As expected, the impact of the impaired AC edges is relatively small when the ZZ edges are highly conductive: the currents in the panes (b) and (c) of Fig. 9 exhibit only a weak dependence on V_A. Cf. discussion to Fig. 4 in Sect. 4.1 concerning the cancellation of intra-GNR current flows. In this way the ZZ edges can serve as two almost uncoupled conductors for DC low-voltage transport. Finally we note that the conditions used for the pane (b) of Fig. 9 do not obey to all of the symmetries (27); cf. the remark near the end of Sect. 4.1.

5 Conclusions

We considered a coupled quantum-classical device consisting of an atomistic model of a nanoribbon (NR) and of two classical branches of circuits with resistances and bias

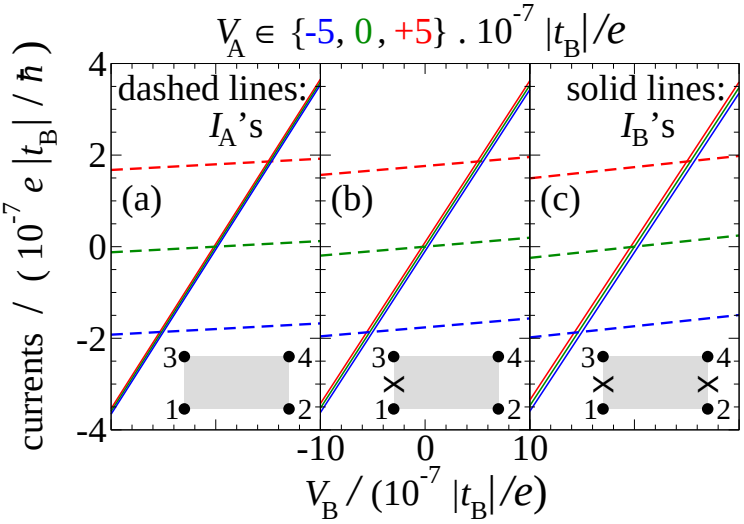

Figure 9: Linear I/V plots analogous to those in Fig. 4 but now the resonantly increased conductance along the ZZ edges is assumed and described by the matrix (38). All other conditions and description are as in Fig. 4 with the exception of the increased scale of the vertical axes. The discussion can be found in Sect. 4.3.

voltage sources. The four electrodes of the circuits have been assumed contacted at the corners of the NR so that the edge-induced modes could be used for the electrical transport. The two bias voltages, not electrochemical potentials, has been assumed as the control variables. In order to analyse the device operation, we have developed a model which allowed us to calculate the two electric currents and three non-trivially dependent electrochemical potentials in the leads as functions of the two externally controlled bias voltages, with the NR's conductance matrix (in general energy dependent) and the classical resistances as given parameters of the model. The model is usable for a general 4-terminal ballistic device and presents a generalisation of the Büttiker's model [7] which assumes zero resistances in the circuits. As a particular material for our computational analysis we assumed graphene. We calculated the conductance matrix using a microscopic theory based on the Green's function matrix formalism. Our present implementation of the formalism allows us to consider graphene nanoribbons (GNRs) up to a size of about 30 000 atoms with computational resources of a desktop personal computer. In the low-voltage linear regime we obtained transparent analytical formulae for the currents $I_{A,B}$ and electrostatic potentials U_α in the system as functions of the applied bias voltages $V_{A,B}$; hence also formulae for the electrochemical potentials $\mu_\alpha = -eU_\alpha$ of the leads. Our formulae for the currents generalise those found by Büttiker in his work [7] for a system with vanishing resistances. Our formulae show how the interplay of the quantum and classical elements of the entire scheme affects the resulting electric currents. Similarly, our formulae for the electrochemical (or electrostatic) potentials at the device's terminals display the non-trivial dependences of the potentials on the classical resistances and on the quantum conductance matrix elements. The analytical

results show that the difference between the electrochemical potentials of a pair of leads (belonging to different circuits) can be tuned to a target value employing a tunable resistor. In this way, the quasi-Fermi level balancing between the leads can be achieved for certain values of the employed physical parameters.

For the voltages in the non-linear regime we developed an efficient numerical algorithm to compute the I/V and μ/V curves. A correction for the non-equilibrium effects has been included.

Our analysis has shown under which conditions the two edges of a nanoribbon behave as two relatively independent wires transporting stationary electric currents. On the other hand, the intriguing regime in which the two classical circuits are significantly coupled through the quantum ballistic device has also been studied: an increase of the voltage (and the current) in one of the circuits induces a substantial change in the current in the other circuit.

Quantitative results have been demonstrated for a GNR with zigzag-edge (ZZ) induced high density of states close to the Fermi level. The system was found to behave similarly to two independent conductors especially for resonantly enhanced conductance along the ZZ edges. For other regimes the mutual interaction of the two associated circuits was found noticeable. Results have been shown for the regimes $1/R_{\mathrm{A,B}} \gg G^{\mathrm{off}}$ and $1/R_{\mathrm{A,B}} \approx G^{\mathrm{off}}$ ($R_{\mathrm{A,B}}$ - the resistances in the classical subsystem, G^{off} - a typical value of an off-diagonal conductance element of the quantum subsystem – the nanoribbon). Although we have considered relatively small GNRs with numbers of atoms of the order of 10^3, our model can be applied to any junction supporting ballistic transport of electrons for which its conductance matrix is know. For example, larger-scale devices such as graphene ribbons used in Ref. [4] could be described as well provided that the conductance matrix could be computed or obtained from experimental measurements.

6 Acknowledgements

This work was supported in parts by the Slovak Research and Development Agency under the contract No. APVV-0108-11 and by the Slovak Grant Agency for Science (VEGA) through grant No. 1/0372/13. Useful discussions with Peter Bokes are acknowledged. The GNR structure was visualised using VMD [19].

Contributions of the authors: P. D. did most of the analysis of the semi-infinite chains eigenstates presented in Sect. A, partially contributed to derive the compact forms (13) of the formulae for the currents and derived the relations (B.19) and (B.20). All other contributions have been done by M. K.

A Eigensystems for semi-infinite chains

Consider a semi-infinite chain of identical equidistantly placed atoms. One explicit orbital $|l\rangle$ per atom at site l is assumed and the independent-electron model is used. Individual lattice sites l (and associated atoms and orbitals) are indexed starting from 1. The orbitals presumably form an orthonormal and complete set:

$$\langle l|l'\rangle = \delta_{ll'} \tag{A.1}$$

and

$$\sum_{l=1}^{\infty} |l\rangle\langle l| = \hat{1} \tag{A.2}$$

The quantum-mechanical description of such a wire then starts with a hamiltonian of the form

$$\hat{H} = \sum_{l=1}^{\infty} \left[\epsilon\, a_l^\dagger a_l + \sum_{m=1}^{N_{\text{far}}} t_m (a_{l+m}^\dagger a_l + a_l^\dagger a_{l+m}) \right] \tag{A.3}$$

where ϵ is the atomic on-site energy (same for each atom) and t_1, t_2, ..., $t_{N_{\text{far}}}$ are the hopping matrix elements, assumed to be negative. $a_l^\dagger$ and a_l are the fermionic creation and annihilation operators, respectively. Each of the eigenstates provided below can be labelled by a unique dimensionless wave-number $\mathcal{K} \in (0, \pi)$. Other values of $\mathcal{K}$ would not yield a physically different eigenstate. The wave-number is related to the eigenenergy through dispersion relation (1). Each of the eigenstates is conveniently expanded in the atomic-orbital basis set:

$$|\psi_{\mathcal{K}}\rangle = \sum_{l=1}^{\infty} \psi_{\mathcal{K},l} |l\rangle \tag{A.4}$$

Each of the three sets provided bellow form a complete eigensystem of states satisfying the condition

$$\langle \psi_{\mathcal{K}} | \psi_{\mathcal{K}'} \rangle = \delta(\mathcal{K} - \mathcal{K}') \tag{A.5}$$

A.1 $N_{\text{far}} = 1$

Eigenstates for this basic tight-binding model are well known and its components in the atomic-orbital basis take the form

$$\psi_{\mathcal{K},l} = \sqrt{\frac{2}{\pi}} \sin(\mathcal{K} l) \tag{A.6}$$

Physically they represent an equally weighted linear combination of an incoming and reflected wave. They form a non-degenerate set.

A.2 $N_{\mathrm{far}} = 2$

Inclusion of 2nd NN interactions complicates the physics of the eigenstates and also their mathematical form. Dispersion relation (1) for this case can be written as

$$\mathcal{E}(\mathcal{K}) = \epsilon - 2t_2 + 2t_1 \cos\mathcal{K} + 4t_2 \cos^2\mathcal{K} \tag{A.7}$$

The energy range $[\mathcal{E}_{\min}, \mathcal{E}_{\max}]$ available to the eigenstates is obtained by running $\mathcal{K}$ over the interval $[0, \pi]$. See also Sect. 2 in the main text. Now we choose any single energy $\mathcal{E} \in [\mathcal{E}_{\min}, \mathcal{E}_{\max}]$ and find all possible inequivalent values of $\mathcal{K}$ which satisfy equation (A.7) for given $\mathcal{E}$. This includes solving a quadratic equation for $\cos\mathcal{K}$. Apart from the real $\pm\mathcal{K}$ (and their periodic replicas) there are also complex wave-numbers found. They give rise to evanescent (or surface) states. We limit our discussion to cases without degeneracy (which is true for all relevant numerical values of t_1 and t_2). The complex wave-number is then found to have a form

$$\hat{\mathcal{K}} = \pi + \mathrm{i}\kappa \tag{A.8}$$

with $\kappa > 0$. Solutions with $-\kappa$ are mathematically correct but they do not satisfy the physical condition that the eigenstates have to be limited. Collecting the knowledge, the amplitudes of any of the physically correct eigenstates can be expressed by the formula

$$\psi_{\mathcal{K},l} = \sqrt{\frac{2}{\pi}} \left[\cos(\mathcal{K}l - \alpha) + (-1)^{l+1} e^{-\kappa l} \cos\alpha\right] \tag{A.9}$$

with

$$\alpha = \arctan\left(\frac{\cos\mathcal{K} + e^{\kappa}}{\sin\mathcal{K}}\right) \tag{A.10}$$

and

$$\kappa = \operatorname{arccosh}[-\cos(\mathcal{K}_-)] \tag{A.11}$$

$$\cos(\mathcal{K}_-) = -\frac{t_1}{4t_2} - \sqrt{\mathcal{D}} \tag{A.12}$$

$$\mathcal{D} = \left(\frac{t_1}{4t_2}\right)^2 + \frac{\mathcal{E} - \epsilon}{4t_2} + \frac{1}{2} \tag{A.13}$$

The ordinary wave-number $\mathcal{K} \equiv \mathcal{K}_+$ (with the sign coming from the associated branch when solving the quadratic equation) is for given $\mathcal{E}$ found from relation

$$\mathcal{K} = \arccos\left(-\frac{t_1}{4t_2} + \sqrt{\mathcal{D}}\right) \tag{A.14}$$

Eigenstates (A.9) form a non-degenerate set.

A.3 $N_{\mathrm{far}} = 3$

We have also implemented the case with hoppings up to the 3rd NN included in the wires. Eigenstates of the semi-infinite wire for typically used values of parameters t_1, t_2, and t_3 now take the form

$$\psi_{\mathcal{K},l} = \sqrt{\frac{2}{\pi}} \left[\cos(\mathcal{K}l + \alpha) + B\cos(ql + \beta)e^{-\kappa l}\right] \tag{A.15}$$

and again are non-degenerate. We do not provide detailed description of the included parameters because the case of $N_{\mathrm{far}} = 3$ is only marginally important for the present work; the effect of the 3rd NN in our study is negligible. Moreover, associated formulas for the parameters are rather lengthy and the components of the wave-numbers are found from solutions of a cubic equation. We mention that the amplitude B is a positive real quantity.

B Solution of the linear equations for the currents and electrostatic potentials

B.1 Conductance matrix G obeying to the time-reversal symmetry only

The linear regime assumed in Sect. 3.3.2 led to the set of 8 linear equations (11), (7), (8), (9a), and (9b) for 7 unknown quantities U_2, U_3, U_4, I_1, ..., I_4. If the circuits conditions (7) and (8) are taken into account, the Eqs. (11) for the 4-terminal device take the form

$$(G_{12} + G_{13} + G_{14})U_1 - G_{12}U_2 - G_{13}U_3 - G_{14}U_4 - I_1 = 0 \tag{B.1}$$

$$-G_{21}U_1 + (G_{21} + G_{23} + G_{24})U_2 - G_{23}U_3 - G_{24}U_4 + I_1 = 0 \tag{B.2}$$

$$-G_{31}U_1 - G_{32}U_2 + (G_{31} + G_{32} + G_{34})U_3 - G_{34}U_4 - I_3 = 0 \tag{B.3}$$

$$-G_{41}U_1 - G_{42}U_2 - G_{43}U_3 + (G_{41} + G_{42} + G_{43})U_4 + I_3 = 0 \tag{B.4}$$

After inclusion of the TRS (4) these four equations are found linearly dependent in a simple manner: adding together first two of them would provide us with the same equation as adding together the second two of them. The Resulting equation, to be used later on, is

$$(G_{31} + G_{41})U_1 + (G_{32} + G_{42})U_2 - (G_{13} + G_{23})U_3 - (G_{14} + G_{24})U_4 = 0 \tag{B.5}$$

We still have available the ground-level condition (10) (see Fig. 2) which we apply now without any relevant loss of generality. We will restore U_1 in our final results. From the Eq. (B.5) we express

$$U_3 = \frac{G_{32}+G_{42}}{G_{13}+G_{23}}\,U_2 - \frac{G_{14}+G_{24}}{G_{13}+G_{23}}\,U_4 \equiv c_2 U_2 - c_4 U_4 \tag{B.6}$$

In the right part of the Eq. (B.6) we have introduced the constants

$$c_2 \equiv \frac{G_{32}+G_{42}}{G_{13}+G_{23}}\,, \qquad c_4 \equiv \frac{G_{14}+G_{24}}{G_{13}+G_{23}}\,. \tag{B.7}$$

We first express currents I_1 and I_3 as some (linear) functions of the two potentials: substitution of the expression (B.6) for U_3 into the Eqs. (B.1) and (B.4) (with $U_1 = 0$) provides us with a pair of linear equations

$$\left(G_{12} + \frac{G_{32}+G_{42}}{G_{13}+G_{23}}\,G_{13}\right) U_2 + \left(G_{14} - \frac{G_{14}+G_{24}}{G_{13}+G_{23}}\,G_{13}\right) U_4 = -I_1 \tag{B.8a}$$

$$\left(G_{42} + \frac{G_{32}+G_{42}}{G_{13}+G_{23}}\,G_{43}\right) U_2 - \left(G_{41}+G_{42}+G_{43} + \frac{G_{14}+G_{24}}{G_{13}+G_{23}}\,G_{43}\right) U_4 = I_3 \tag{B.8b}$$

i.e. we now have available explicit formulae

$$I_1 = I_1(U_2, U_4)\,, \qquad I_3 = I_3(U_2, U_4)\,. \tag{B.9}$$

From this point we switch the notation for currents and to use I_A instead of $-I_1 = I_2$ and I_B instead of $-I_3 = I_4$:

$$I_\mathrm{A} \equiv I_2\,, \quad I_\mathrm{B} \equiv I_4 \tag{B.10}$$

The externally controllable mutually independent variables are the two bias voltages V_A and V_B, not the potentials U_2, U_4. There are also the two resistors in the circuits. Our aim is to find the electric currents I_A and I_B flowing through the leads at the terminals 2 and 4 as functions of the bias voltages V_A and V_B. To accomplish the goal we relate the potentials U_2 and U_4 to the bias voltages V_A and V_B using the Kirchhoff's second law (9). Relation (9b) for U_4 includes potential U_3 which is another unknown variable and has to be expressed as $U_3 = U_3(U_2, U_4)$ using (B.6). Accomplishing this calculation we obtain an expression for U_4 which we put down together with the Eq. (9a) for U_2, now simplified due to the choice (10).

$$U_2 = V_\mathrm{A} - R_\mathrm{A} I_\mathrm{A} \tag{B.11a}$$

$$U_4 = \frac{1}{1+c_4}\left(c_2 V_\mathrm{A} - c_2 R_\mathrm{A} I_\mathrm{A} + V_\mathrm{B} - R_\mathrm{B} I_\mathrm{B}\right) \tag{B.11b}$$

These forms will be inserted into the linear set (B.8). To do this, we introduce another abbreviated notation: the linear set (B.8) will be written as

$$aU_2 + bU_4 = I_{\rm A} \tag{B.12a}$$
$$cU_2 - dU_4 = -I_{\rm B} \tag{B.12b}$$

where

$$a \equiv G_{12} + \frac{G_{32}+G_{42}}{G_{13}+G_{23}}\,G_{13} \equiv\ G_{12} + c_2 G_{13} \tag{B.13a}$$
$$b \equiv G_{14} - \frac{G_{14}+G_{24}}{G_{13}+G_{23}}\,G_{13} \equiv\ G_{14} - c_4 G_{13} \tag{B.13b}$$
$$c \equiv G_{42} + \frac{G_{32}+G_{42}}{G_{13}+G_{23}}\,G_{43} \equiv\ G_{42} + c_2 G_{43} \tag{B.13c}$$
$$d \equiv \qquad\qquad\qquad\qquad \equiv\ G_{41} + G_{42} + (1+c_4)G_{43} \tag{B.13d}$$

Now we accomplish the substitution of (B.11) into the abbreviated linear set (B.12):

$$a(V_{\rm A} - R_{\rm A}I_{\rm A}) + b\left[\frac{1}{1+c_4}\,(c_2 V_{\rm A} - c_2 R_{\rm A} I_{\rm A} + V_{\rm B} - R_{\rm B} I_{\rm B})\right] = I_{\rm A} \tag{B.14a}$$
$$c(V_{\rm A} - R_{\rm A}I_{\rm A}) - d\left[\frac{1}{1+c_4}\,(c_2 V_{\rm A} - c_2 R_{\rm A} I_{\rm A} + V_{\rm B} - R_{\rm B} I_{\rm B})\right] = -I_{\rm B} \tag{B.14b}$$

After regrouping of the terms and denoting

$$\frac{1}{1+c_4} \equiv c_4' \tag{B.15}$$

we obtain

$$[1 + (a + bc_4'c_2)R_{\rm A}]\,I_{\rm A} + \qquad bc_4' R_{\rm B} I_{\rm B} = \quad (a + bc_4'c_2)V_{\rm A} + bc_4' V_{\rm B} \tag{B.16a}$$
$$(-c + dc_4'c_2)R_{\rm A} I_{\rm A} + (1 + dc_4' R_{\rm B})I_{\rm B} = (-c + dc_4'c_2)V_{\rm A} + dc_4' V_{\rm B} \tag{B.16b}$$

Solving this pair of the linear equations for the unknown currents $I_{\rm A}$ and $I_{\rm B}$ we get linear relations

$$I_{\rm A} = I_{\rm A}(V_{\rm A}, V_{\rm B})\,, \qquad I_{\rm B} = I_{\rm A}(V_{\rm A}, V_{\rm B}) \tag{B.17}$$

Accomplishing series of algebraic manipulations with multiple use of the TRS relations

$$\sum_{\beta(\neq\alpha)} G_{\alpha\beta} = \sum_{\beta(\neq\alpha)} G_{\beta\alpha} \tag{B.18}$$

we finally obtain explicit formulae (13) displayed in the main text. The determinant of the left hand side of the linear system (B.16) is actually the expression $D(G,R)$ given

by the Eq. (21). We find that the Büttiker's conductances $\alpha_{CC'}$ can alternatively be expressed by formulae

$$\alpha_{\mathrm{AA}} = S_1 \quad - \frac{1}{S}\,(S_1 - G_{12})(S_1 - G_{21}) \tag{B.19a}$$

$$\alpha_{\mathrm{AB}} = G_{13} - \frac{1}{S}\,(S_1 - G_{12})(S_3 - G_{43}) \tag{B.19b}$$

$$\alpha_{\mathrm{BA}} = G_{31} - \frac{1}{S}\,(S_1 - G_{21})(S_3 - G_{34}) \tag{B.19c}$$

$$\alpha_{\mathrm{BB}} = S_3 \quad - \frac{1}{S}\,(S_3 - G_{34})(S_3 - G_{43}) \tag{B.19d}$$

and satisfy the relation

$$(\alpha_{\mathrm{AA}} - S_1)(\alpha_{\mathrm{BB}} - S_3) = (\alpha_{\mathrm{AB}} - G_{13})(\alpha_{\mathrm{BA}} - G_{31}) \tag{B.20}$$

B.2 The special case with 4 independent matrix elements of G

We now assume the simplifying relations (27) of Sect. 3.3.3. To obtain the currents under these higher-symmetry conditions, we could start from the general results (13) and simplify them using the expressions (28). Instead we follow here a different convenient route and derive the results as given below. Constants c_2 and c_4, according to their definitions (B.7), become

$$c_2 = c_4 = 1 \tag{B.21}$$

which will obviously greatly simplify the remaining derivation. The equation pair (B.8) then becomes

$$(G_{12} + G_{13})\,U_2 + \qquad (G_{14} - G_{13})\,U_4 = -I_1 \tag{B.22a}$$

$$(G_{12} + G_{13})\,U_2 - (G_{14} + G_{13} + 2G_{12})\,U_4 = \quad I_3 \tag{B.22b}$$

and from the Eq. (B.6) we also have a simplified formula for U_3 valid for $U_1 = 0$:

$$U_3 = U_2 - U_4 \tag{B.23}$$

Next, the circuit relations (B.11) reduce to the form

$$U_2 = V_{\mathrm{A}} - R_{\mathrm{A}} I_{\mathrm{A}} \tag{B.24a}$$

$$U_4 = \frac{1}{2}\,(V_{\mathrm{A}} - R_{\mathrm{A}} I_{\mathrm{A}} + V_{\mathrm{B}} - R_{\mathrm{B}} I_{\mathrm{B}}) \tag{B.24b}$$

With the help of the notation defined by the Eqs. (27) the four auxiliary constants (B.13) now reduce to

$$\begin{aligned} a = c &= D + E \\ b &= F - E \\ d = 2a + b &= 2D + E + F \end{aligned} \tag{B.25}$$

and finally the linear set (B.16) becomes

$$[2 + dR_\mathrm{A}]\, I_\mathrm{A} + \qquad bR_\mathrm{B}\, I_\mathrm{B} = d\, V_\mathrm{A} + b\, V_\mathrm{B} \tag{B.26a}$$

$$bR_\mathrm{A}\, I_\mathrm{A} + (2 + dR_\mathrm{B})\, I_\mathrm{B} = b\, V_\mathrm{A} + d\, V_\mathrm{B} \tag{B.26b}$$

Upon solving the equations we obtain the explicit formulae (29) shown in main text.

C Solution of the non-linear equations for the currents and electrochemical potentials

In Sects. 2 and 3.3.1 the scheme according to Fig. 2 have been defined. The solution to the corresponding equations in the linear regime was found in Sect. 3.3.2 and in appendix B. In Sect. 3.3.4 we described how the task is solved in the non-linear regime where the full dependence of the transmission matrix on the energy has to be taken into account. Here we provide additional details of this procedure. Like in the linear regime (c.f. the Eqs. (B.16)) we now obtain equations

$$[1 + (a + bc_4' c_2)R_\mathrm{A}]\, \delta I_\mathrm{A} + \qquad bc_4' R_\mathrm{B}\, \delta I_\mathrm{B} \quad = (a + bc_4' c_2)\, \delta V_\mathrm{A} + bc_4'\, \delta V_\mathrm{B} \tag{C.1a}$$

$$(-c + dc_4' c_2)R_\mathrm{A}\, \delta I_\mathrm{A} + (1 + dc_4' R_\mathrm{B})\, \delta I_\mathrm{B} = (-c + dc_4' c_2)\, \delta V_\mathrm{A} + dc_4'\, \delta V_\mathrm{B} \tag{C.1b}$$

which have their structure identical to the Eqs. (B.16). Various coefficients in the Eqs. (C.1) now include the conductance matrix elements at three different energies indicated by the superscript:

$$c_2 \equiv \frac{G_{32}^{(2)} + G_{42}^{(2)}}{G_{13}^{(3)} + G_{23}^{(3)}}\,, \qquad c_4 \equiv \frac{G_{14}^{(4)} + G_{24}^{(4)}}{G_{13}^{(3)} + G_{23}^{(3)}}\,. \tag{C.2}$$

$$a \equiv G_{12}^{(2)} + \frac{G_{32}^{(2)} + G_{42}^{(2)}}{G_{13}^{(3)} + G_{23}^{(3)}} G_{13}^{(3)} \equiv G_{12}^{(2)} + c_2 G_{13}^{(3)} \tag{C.3a}$$

$$b \equiv G_{14}^{(4)} - \frac{G_{14}^{(4)} + G_{24}^{(4)}}{G_{13}^{(3)} + G_{23}^{(3)}} G_{13}^{(3)} \equiv G_{14}^{(4)} - c_4 G_{13}^{(3)} \tag{C.3b}$$

$$c \equiv G_{42}^{(2)} + \frac{G_{32}^{(2)} + G_{42}^{(2)}}{G_{13}^{(3)} + G_{23}^{(3)}} G_{43}^{(3)} \equiv G_{42}^{(2)} + c_2 G_{43}^{(3)} \tag{C.3c}$$

$$d \equiv \equiv G_{41}^{(4)} + G_{42}^{(4)} + (1 + c_4) G_{43}^{(3)} \tag{C.3d}$$

c_4' used in the Eqs. (C.1) is again defined by the expression (B.15) but now with the more general c_4 according to the Eq. (C.2). The precise meaning of the superscript notation is defined by

$$G_{\alpha\beta}^{(\gamma)} \equiv \frac{2e^2}{h} \mathcal{T}_{\beta\to\alpha}(\mu_\gamma) \tag{C.4}$$

i.e. the upper index of $G_{\alpha\beta}$ marks the value of the electrochemical potential at which the conductance has to be evaluated.

If we now, for a fixed set of known functions $G_{\alpha\beta}(u)$, aim to calculate the currents I_A and I_B at given bias voltages V_A and V_B, we start from zero voltages and in small steps δV_A and δV_B increase them up to their final values V_A and V_B. The path in the $(V_\mathrm{A}, V_\mathrm{B})$ space can be arbitrary. The procedure is numerically stable for all examined cases and requires almost negligible computational time in comparison to that used to compute the spectra of $G_{\alpha\beta}(u)$.

References

[1] K. Nakada, M. Fujita, G. Dresselhaus and M.S. Dresselhaus, *Phys. Rev. B* **54**, 17954 (1996).

[2] O.V. Yazyev and M.I. Katsnelson, *Phys. Rev. Lett.* **100**, 047209 (2008).

[3] W. Yao, S.A. Yang and Q. Niu, *Phys. Rev. Lett.* **102**, 096801 (2009).

[4] M.T. Allen O. Shtanko, I.C. Fulga, A.R. Akhmerov, K. Watanabe, T. Taniguchi, P. Jarillo-Herrero, L.S. Levitov and A. Yacoby, *Nature Physics* **12**, 128 (2016).

[5] X. Wang, Y. Ouyang, X. Li, H. Wang, J. Guo and H. Dai, *Phys. Rev. Lett.* **100**, 206803 (2008).

[6] M. Konôpka, J. Phys.: Condens. Matter. **27**, 435005 (2015).

[7] M. Büttiker, *Phys. Rev. Lett.* **14**, 1761 (1986).

[8] R. de Picciotto, H.L. Stormer, L.N. Pfeiffer, K.W. Baldwin and K.W. West, *Nature* **411**, 51 (2001).

[9] Diwakar Ramamurthy and C.H. Wu, *Phys. Rev. B* **66**, 115307 (2002).

[10] J. Gabelli, G. Fève, J.-M. Berroir, B. Plaçais, A. Cavanna, B. Etienne, Y. Jin and D.C. Glattli, *Science* **313**, 499 (2006).

[11] J. Gabelli, G. Fève, J.-M. Berroir and B. Plaçais, *Rep. Prog. Phys.* **75**, 126504 (2012).

[12] S. Wang, L. Talirz, C.A. Pignedoli, X. Feng, K. Müllen, R. Fasel and P. Ruffieux, *Nature Commun.* **7**, 11507 (2016).

[13] S. Reich, J. Maultzsch, C. Thomsen and P. Ordejón, *Phys. Rev. B* **66**, 035412 (2002).

[14] O.V. Yazyev, *Rep. Prog. Phys.* **73**, 056501 (2010).

[15] M. Konôpka and P. Bokes, *Phys. Rev. B* **89**, 125424 (2014).

[16] D.A. Ryndyk, B. Song, R. Gutiérrez and G. Cuniberti, *Green Function Techniques in the Treatment of Quantum Transport at the Molecular Scale*, in *Energy Transfer Dynamics in Biomaterial Systems, edited by I. Burghardt, V. May, D.A. Micha and E. Bittner*, Springer Series in Chemical Physics Vol. 93 (Springer-Verlag, Berlin, Heidelberg, 2009), p. 213.

[17] D.A. Areshkin, D. Gunlycke and C.T. White, *Nano Lett.* **7**, 204 (2007).

[18] Quantitatively, an edge defect is not likely to totally suppress the conductance G_{13} neither to leave the other matrix elements unaffected; hence our example with $G_{13} \approx 0.003\,G_0$ represents a qualitative and simplified description of the edge disorder impact in terms of a model situation. In order to acquire a quantitative estimate of the magnitude of the edge defects on the conductance, we accomplished a few quantum-mechanical calculations of perturbed GNRs. For example, a structure with one C-C-C group (i.e. 3 carbon atoms) removed from the left-hand side AC edge of the GNR in Fig. 1 yielded matrix elements $12 : 0.1676$, $13 : 0.0652$, $14 : 0.1677$, $23 : 0.0155$, $24 : 0.0388$ and $34 : 0.0140$, all in units of G_0. These quantities should be compared to the matrix (35). We note that even slightly different defects may lead to significantly different conductance matrices. The numbers of this particular example display the notably decreased G_{13} matrix element and the pronounced asymmetry between G_{14} and G_{23}.

[19] W. Humphrey, A. Dalke and K. Schulten, *J. Molec. Graphics* **14**, 33 (1996).